Author's Accepted Manuscript

www.elsevier.com/locate/memsci

Development of advanced nanocomposite membranes using graphene nanoribbons and nanosheets for water treatment

Amin Karkooti, Alireza Zehtab Yazdi, Pu Chen, Mick McGregor, Neda Nazemifard, Mohtada Sadrzadeh

PII: S0376-7388(18)30307-7
DOI: https://doi.org/10.1016/j.memsci.2018.04.034
Reference: MEMSCI16118

To appear in: *Journal of Membrane Science*

Received date: 16 March 2018
Revised date: 18 April 2018
Accepted date: 22 April 2018

Cite this article as: Amin Karkooti, Alireza Zehtab Yazdi, Pu Chen, Mick McGregor, Neda Nazemifard and Mohtada Sadrzadeh, Development of advanced nanocomposite membranes using graphene nanoribbons and nanosheets for water treatment, *Journal of Membrane Science,* https://doi.org/10.1016/j.memsci.2018.04.034

Development of advanced nanocomposite membranes using graphene nanoribbons and nanosheets for water treatment

Amin Karkooti[1], Alireza Zehtab Yazdi[2], Pu Chen[2], Mick McGregor[3], Neda Nazemifard[1], Mohtada Sadrzadeh[4]*

[1]Department of Chemical & Materials Engineering, 12-237 Donadeo Innovation Centre for Engineering, University of Alberta, Edmonton, AB, Canada, T6G 1H9
[2]Department of Chemical Engineering, University of Waterloo, 200 University Avenue West, Waterloo, Ontario, Canada, N2L3G1
[3]Suncor Energy Inc., P.O. Box 2844, 150-6th Ave. SW, Calgary, Alberta, Canada T2P 3E3
[4]Department of Mechanical Engineering, 10-367 Donadeo Innovation Center for Engineering, Advanced Water Research Lab (AWRL), University of Alberta, Edmonton, AB, Canada, T6G 1H9
* Corresponding Author: sadrzade@ualberta.ca; Tel. +1 780-492-8745

Abstract

Water-intensive industries have to comply with stringent environmental regulations and evolving regulatory frameworks requiring the development of new technologies for water recycling. Development of polymeric membranes may provide an effective solution to improve water recycling, but require finely-tuned pore size and surface chemistry for ionic and molecular sieving to be efficient. Additionally, fouling is a major challenge that limits the practical application of the membranes in water recycling in these industries. In this work, four different graphene oxide (GO) derivatives were incorporated into a polyethersulfone (PES) matrix *via* a non-solvent induced phase separation (NIPS) method. The GO derivatives used have different shapes (nanosheets *vs* nanoribbons) and different oxidation states (C/O=1.05-8.01) with the potential to enhance water flux and suppress fouling of the membranes through controlled pore size, hydrophilicity, and surface charge. The permeation properties of the PES/GO membranes were evaluated using a water sample from the Athabasca oil sands of Alberta. The results for contact angle and streaming potential measurements indicate the formation of more hydrophilic and negatively charged PES/GO nanocomposite membranes. All graphene-based nanocomposite membranes demonstrated better water flux and rejection of organic matter compared to the unmodified PES membrane. The fouling measurement results revealed that fouling was impeded due to enhanced membrane surface properties. Longitudinally unzipped graphene oxide nanoribbons (GONR-L) at an optimum

loading of 0.1 weight percent (wt.%) provided the maximum water flux (70 LMH at 60 psi), organic matter rejection (59%) and antifouling properties (30% improvement compared to pristine PES membrane). Flux recovery ratio experiments indicated a remarkable enhancement in the fouling resistance property of PES/GO nanocomposite membranes.

Keywords: Graphene oxide, Graphene nanoribbon, nanocomposite membranes, oil sands, produced water treatment

1. Introduction

Improved water usage efficiency has driven the research community to explore advanced methods for water recycling that are more environmentally sustainable and energy efficient [1]. Filtration using polymeric membranes has attracted attention due to the ease of operation and integration with other processes, reliable contaminant removal without production of any harmful by-products, and cost efficiency, compared to other conventional filtration technologies [2,3].

Polyethersulfone (PES) has been extensively used for applications in ultrafiltration (UF) and nanofiltration (NF) systems, where it can offer superior mechanical strength, chemical and thermal stabilities and a wide range of pH resistance [4]. PES, however, is inherently fairly hydrophobic, which could lead to severe fouling in long-run operations. Throughout the fouling process, the key membrane properties, i.e., water permeation and solute rejection rate, are affected that ultimately increase the operating cost, and decrease the membrane lifespan [5].

Surface properties of polymeric membranes can have significant impacts on the initial stages of fouling where the negatively-charged and hydrophilic surfaces can effectively hinder the fouling process [8-10]. As a result, membrane cleaning interval can be prolonged. Numerous studies have investigated surface properties and morphologies of the polymeric membranes with the objective to fabricate fouling-resistant surfaces against different kinds of foulants [5,8–11]. Several approaches have been explored, such as surface coating [12,13], chemical grafting [14], ultraviolet-assisted plasma treatment [15,16], and physical blending with antifouling materials [17].

Incorporation of hydrophilic nanofillers into the polymer matrix to fabricate polymer nanocomposite membranes is one of the most effective approaches that showed promising potentials for surface modification [11]. This technique has the advantage of being straightforward and cost-effective and can enhance antifouling properties, selectivity, and thermomechanical stability of membranes [18].

Various studies explored the effect of incorporating a broad category of nanofillers including single-element oxides (TiO_2 [19,20], ZrO_2 [21–23], MgO [24], Al_2O_3 [25], SiO_2 [26,27], Fe_2O_3 [28]), double-element oxides (indium tin oxide, ITO [29]), molecular-sieve nanomaterials (zeolites [30]), and carbon-based nanomaterials (carbon nanotube [31,32], cellulose nanocrystals (CNC) [33], and graphene oxide (GO) [2,34]) into polymer membrane matrix. Recently, graphene-based nanomaterials have emerged as a topic of vast scientific interest [35–38]. These nanomaterials are carbon allotropes composed of a monolayer of tightly packed carbon atoms with various geometrical structures, e.g., nanosheets, nanoribbons, and nanotubes [39]. Graphene-based nanomaterials can also be readily synthesized with different functional groups, e.g., carboxyl, epoxy, and hydroxyl, positioned at their edges and basal planes. Two exceptional properties of these nanomaterials have made them attractive for the development of nanocomposite membranes. First, most of GO derivatives have high charge density that help reaching stable dispersion in organic solutions (e.g., DMAc solution) [40]. Second, due to different oxidation state, they possess tunable hydrophilic properties that can be induced to the polymer material and high-performance membranes can be fabricated in terms of flux and antifouling properties to satisfy specific water treatment applications.

A summary of earlier studies on the effect of incorporating GO nanofillers on membrane properties is presented in Table 1. As can be observed, the addition of GO nanofillers has generally improved mechanical, permeation, and antifouling properties of polymer membranes. However, these results were primarily based upon utilization of GO nanosheets with specific geometrical and chemical characteristics, and the effect of shape and oxidation state of nanofillers on membrane properties yet to be explored.

Table 1: Brief overview of previous studies on the effect of GO on membrane properties

Reference	Additive	Polymer	Major finding
Ganesh et al. [34]	GO	PSf[1]	Increase in pure water flux and salt rejection
Yu et al. [41]	HPEI[2]-GO	PES	Lower permeation but improved tensile strength and antifouling properties
Lee et al. [42]	GO	PSf	Enhanced antifouling ability of the developed membrane bioreactor (MBR)
Zhao et al. [43]	GO	PVC[3]	Significant enhancement in hydrophilicity, water flux, and mechanical properties
Wu et. al. [44]	SiO_2-GO	PSf	Enhanced permeation and protein rejection and anti-fouling ability
Lim et al. [45]	TA[4]-GO	PEI[5]	Excellent antibacterial activity against E. Coli
Zinadini et. al.[4]	GO	PES	Improved water flux, dye removal, and anti-biofouling properties
Xu et al. [46]	Organosilane - GO	PVDF[6]	Enhanced mechanical strength, permeation and flux recovery ratio (FRR)

[1]Polysulfone, [2]Hyperbranched polyethylenimine, [3]Polyvinyl chloride, [4]Tannic acid, [5]Polyethylenimine, [6]Polyvinylidene fluoride

In the present work, we report the effect of incorporation of four GO derivatives on physicochemical characteristics and permeation properties of the polyethersulfone (PES) membranes. The GO derivatives used in this study include graphene nano-platelet (GNP), graphene oxide (GO) nano-sheet, longitudinally unzipped graphene oxide nano-ribbon (GONR-L), and helically unzipped graphene oxide nano-ribbon (GONR-H). They have different shapes and oxidation states with the potentials to enhance water flux and fouling resistance of the nanocomposite membranes through controlled surface charge density, and hydrophilicity of membrane surface. The nanocomposite membranes were fabricated *via* non-solvent phase separation (NIPS) method. Structural morphology, surface properties, and chemical composition of fabricated membranes were examined by field emission scanning electron microscopy (FESEM), Fourier-transform infrared spectroscopy (FTIR), water contact angle, and surface zeta potential measurements. Water flux, rejection of organic matter and fouling resistance of the synthesized nanocomposite membranes were studied using synthetic and real produced water and was compared with unmodified PES membrane.

2. Materials and Methods

2.1. Chemical and reagents

PES was obtained from BASF and was used to prepare porous UF membranes. N,N-dimethylacetamide (DMAc), potassium permanganates, and H_2SO_4 were purchased from Fisher Scientific. Graphene nanoplatelets (GNP) and GO were supplied from Carbon Upcycling Technologies (CUT). The fluids used for testing fouling on the membrane were SAGD produced water samples provided from a SAGD water treatment plant located in the Athabasca oil sands region of Alberta. The GONR-L and GONR-H were synthesized by using the previously reported carbon nanotube unzipping procedure where multiwalled carbon nanotubes were treated with potassium permanganates in acid [47–51].

2.2. Preparation of GO/PES nanocomposite membranes

GO/PES membranes were fabricated via NIPS method. This process relies on the phase separation of a polymer solution, producing a porous polymer film. Homogeneous polymer solutions were prepared by mixing DMAc with 18 wt.% PES, 2 wt.% PVP, and different ratio of GO derivatives to polymer (0.05, 0.1, 0.2 wt.%) shown in Table 2. To prepare a casting solution, first GO nanofillers were uniformly dispersed in DMAc using a probe sonicator for 15 minutes. Then, PES and PVP were added to GO-DMAc mixture and stirred overnight. The solution was then kept still for 24 h at room temperature for the complete removal of the air bubbles from the solution. After that, the polymer solution was cast on the flat glass surface using a film applicator (Gardco, MICROM II) with casting speed of 5 mm/s and the clearance gap of 150 microns. Finally, the cast film was immersed in a water bath for 24 hours to complete membrane formation by liquid-liquid demixing.

Table 2: Concentration of GO nanofillers in the polymer casting solution

Membrane	Nanofiller	The ratio of nanofiller to polymer
M0	---	0
M1	GNP	0.05
M2	GNP	0.1
M3	GNP	0.2
M4	GO	0.05
M5	GO	0.1
M6	GO	0.2
M7	GONR-L	0.05
M8	GONR-L	0.1

M9	GONR-L	0.2
M10	GONR-H	0.05
M11	GONR-H	0.1
M12	GONR-H	0.2

2.3. Measurement of porosity and pore size

Porosity is the ratio of the total pore volume to the volume of the membrane. The gravimetric method was used to evaluate average porosity (ε) of membranes [52]:

$$\varepsilon = \frac{w_1 - w_2}{(A \times l)\rho} \qquad (1)$$

where w_1 and w_2 are the mass of wet and dry membranes (g), respectively; A is the membrane surface area (cm^2), l is the membrane thickness (cm), and ρ is the water density (0.997 g/cm^3 at 25 °C). All measurements were repeated at least 3 times and the average value were reported as the membrane porosity.

To measure the membrane average pore size, the relationship proposed by Guerout-Elford-Ferry [4] is used:

$$r_{\mathrm{m}} = \sqrt{\frac{(2.9 - 1.75\varepsilon)8\eta l Q}{\varepsilon \times A \times \Delta P}} \qquad (2)$$

where η is the water viscosity (8.9×10^{-4} Pa.S at 25°C), Q is the permeate volumetric flow rate (m^3/s), and ΔP is the transmembrane pressure (Pa). The operational transmembrane pressure is 0.28 MPa (40 psi).

2.4. Pure water flux measurement

Pure water flux experiments were conducted using a lab-scale batch filtration setup consists of a dead-end stirred cell (Amicon, UFSC40001) with the capacity of 400 ml and effective membrane area of 41.8 cm^2. Pressurized nitrogen gas was used to apply 40 psi pressure. A digital balance (ME4002, Mettler Toledo, USA) connected to a computer was used to automatically monitor and record the permeate water flux over time. The fabricated membranes were immersed in water for 24 hours and then were compacted at 70 psi for 1 hour before each permeation test to achieve a steady flux. During filtration, the feed solution was stirred at a rate of 300 rpm. The following equation was used to calculate the water flux (J_0):

$$J_0 = \frac{W}{A \times \Delta t} \quad (3)$$

where W is the mass of the permeate water (kg), A is the membrane effective area (m^2), and Δt is the permeation time (h).

2.5. Produced water treatment

To evaluate the separation performance of the synthesized membranes filtration experiments were conducted on WLS inlet water of SAGD operation. The concentration of contaminants in the WLS inlet water was determined by ICP-OES (Thermo Scientific, iCAP™ 7400, Massachusetts, USA) and TOC analyzer (Shimadzu, model TOC-V; detection range 3-25,000 mg/L, Kyoto, Japan) and the results are presented in Table 3. The rejection of organic matter by membranes was calculated by measuring the TOC in the collected permeate during the filtration of WLS inlet water at 25˚ C and 40 psi using the following equation:

$$\text{Rejection } (\%) = (1 - \frac{C_p}{C_f}) \times 100 \quad (4)$$

where C_p and C_f are the TOC content in permeate and feed solution, respectively.

2.6. Fouling tests

To investigate fouling behavior of membranes a three-step experimental protocol was followed. First, the pure water flux, J_{W1}, was measured. Then, the water flux during filtration of WLS inlet water, J_{Wf}, was recorded. After hydraulic washing of the membrane surface with deionized water for 10 min, the pure water flux of cleaned membrane, J_{W2}, was measured again. To determine the antifouling property of the membranes total fouling ratio (DR_t) and flux recovery ratio (FRR) were calculated as follows [41]:

Table 3: Properties of WLS inlet water

Parameters	WLS Inlet Water
pH	7.0
TOC (mg/L)	550
TDS(mg/L)	1050
Conductivity (µS/cm)	1508
Na^+ (mg/L)	310
Cl^- (mg/L)	240

Mg^{2+} (mg/L)	0.371
Ca^{2+} (mg/L)	2.83
Iron, total (mg/L)	1.02
SiO_2, dissolved (mg/L)	63.7

$$DR_t = 1 - \frac{J_{Wf}}{J_{W1}} \quad (5)$$

$$FRR = \frac{J_{W2}}{J_{W1}} \quad (6)$$

Here, DR_t is the sum of irreversible fouling ratio (DR_{ir}) and reversible fouling ratio (DR_r) which are associated with the flux decline due to the adsorption of foulant molecules on a membrane surface and concentration polarization phenomenon, respectively. DR_{ir} and DR_r can be calculated by following equations:

$$DR_{ir} = 1 - \frac{J_{W2}}{J_{W1}} \quad (7)$$

$$DR_r = \frac{(J_{W2} - J_{Wf})}{J_{W1}} \quad (8)$$

2.5. Polymer solution viscosity measurement

The viscosity of the polymer solution was measured by Rheometer (Brookfield, DV-III Altra, Massachusetts, USA). The relationship between viscosity and shear rate for each casting solution was acquired at a shear rate ranging from 50 to 250 s^{-1} at 25 ˚C.

2.6. Chemical composition tests

Potassium bromide-Fourier transform infrared (KBr-FTIR) spectroscopy was used to provide information on the type of functional groups present in GO derivatives. The FTIR spectra were obtained using FTIR imaging system (Varian Digitlab, FTS 7000, Massachusetts, USA). This device is equipped with a mercury-cadmium-telluride (MCT) detector with high photometric accuracy and sensitivity. The KBr-FTIR spectroscopy exploits the property of KBr that forms a transparent sheet in infrared region when subjected to high pressure. To prepare 13 mm- diameter pellets, approximately 1% samples of GO nanomaterials mixed with fine moisture-free KBr were

put into the pellet-forming die. A force of about 8000 psi was applied for several minutes to create transparent pellets. The background was measured using pure KBr pellets. All samples were scanned over the range of 600- 4000 cm^{-1} and 100 scans were averaged for each spectral measurement.

Detailed elemental and chemical bonding analysis of GO derivatives was conducted using X-ray photoelectron spectroscopy (XPS). XPS analysis provided information about the outer 1-10 nm of GO derivative samples. In the present work, XPS imaging spectrometer (Kratos, AXIS Ultra, Manchester, UK), equipped with a monochromatic Al Kα X-ray source were used. Low-resolution survey scans, as well as a high-resolution scan of C, were taken. Survey spectra were obtained with a pass energy of 160 eV, and sweep time of 100 s in the range of 0- 1100 eV. High-resolution spectra were obtained for C 1sand then were analyzed using CasaXPS software.

2.7. Surface properties (wettability and surface charge)

Water contact angle on the flat sheet membranes was measured to investigate the surface wetting characteristic of fabricated membranes as a function of GO contents. The measurement was carried out based on sessile drop method using goniometer Kruss Model DSA 100E (Hamburg, Germany) with deionized water. The higher the surface wettability, the lower is the contact angle. For each sample, five measurements were performed, and the average was reported.

The surface zeta potential of the fabricated membranes was measured using Surpass3 analyzer (Anton Paar, Graz, Austria). This device evaluates the surface zeta potential based on streaming potential and streaming current measurements. The zeta potential values were determined at pH 7.0 and 25 ˚C using 0.001 M KCl solution.

2.8. Membranes morphology study

To study the effects of GO content on membranes microstructure, the morphology of fabricated membranes was examined using field emission scanning electron microscopy (FESEM). The dried membranes samples were fractured under liquid nitrogen and were mounted on SEM stub. To improve electron conductivity of the samples 8 nm gold Au was sputter-coated on the surface of

the membranes using Gatan 682 Precision Etching and Coating System (Gatan, Inc., Pleasanton, USA). The cross-sectional images were taken at 5 kV and high vacuum condition.

3. Results and discussion

3.2. FTIR measurement results

FTIR measurement results on the GO derivatives is shown in . 1. The peak at 3435 cm^{-1} is attributed to the OH stretching vibrations in carboxylic groups. The transmittance bands at 1625 cm^{-1} is ascribed to C=C in benzene rings, and sharp, intense peak at 1718 cm^{-1} is attributed to C=O carboxylic groups. The peaks at 1396 cm^{-1}, 1193 cm^{-1}, and 1016 cm^{-1} are attributed to C-O single bond and C=O double bond vibrations. Finally, the peak at 890 cm^{-1} is ascribed to aromatic sp^2 C-H bending. All these groups are valid and are expected to be present in the structure of GO derivatives. GO, GONR-L, and GONR-H possess the same molecular groups, but it seems to differ in chemical makeup (oxidation state). On the contrary, GNP showed smaller peaks for C-O and carboxylic C=O and less intense peak for carboxylic groups. It reveals that GNP has a few epoxides (O-C-O) and hydroxyl groups (C-OH) and confirms that GO, GONR-L, and GONR-H are effectively functionalized.

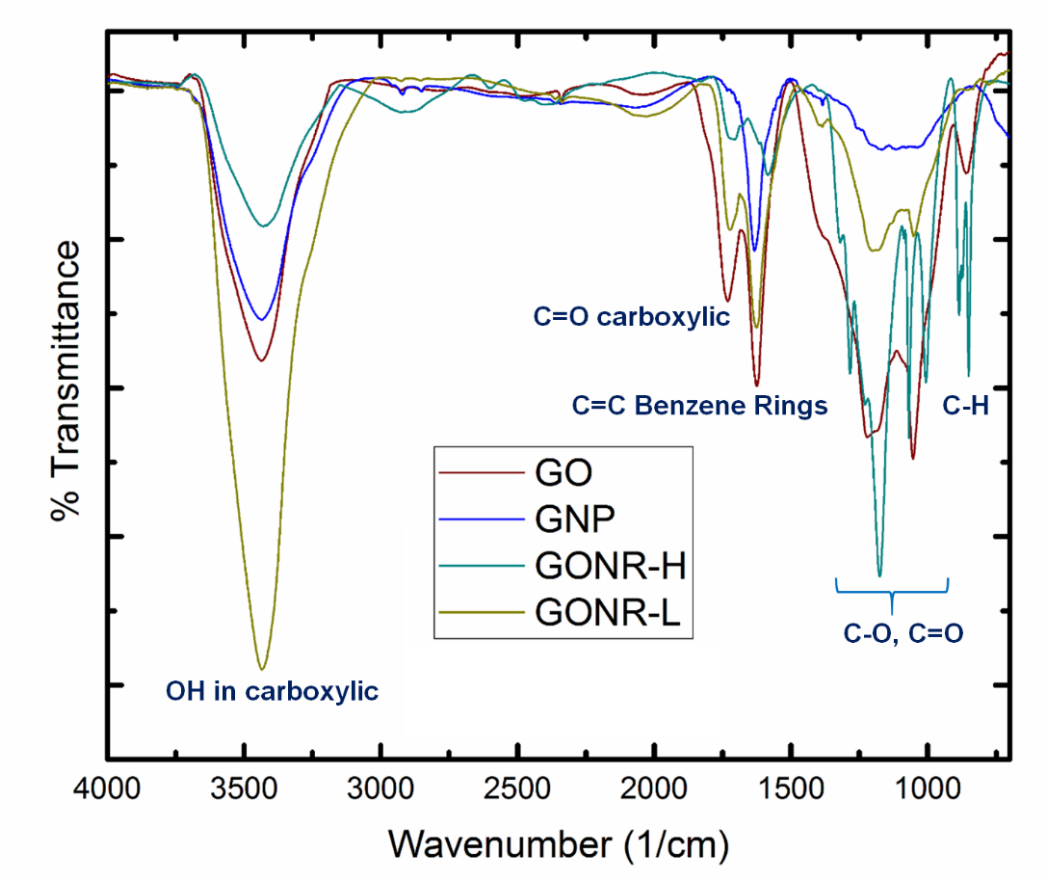

Figure 1: The FTIR spectra of different graphene-based nanomaterials

3.2. XPS Characterization of Graphene Nanofillers

To further investigate the functional state of oxygen existing on the surface of nanofillers XPS analysis was conducted. The survey scans for GNP, GO, GONR-L and GONR-H are presented in Fig. 2. The analysis of survey spectra showed that oxygen functional groups on GONR-H (C/O = 3.10), GO (C/O = 2.04), and GONR-L (C/O = 1.05) were significantly higher than that in GNP (C/O = 8.01). The magnified Survey scan is presented in Figure S3 in Supporting Information. High-resolution C 1s spectra of the GNP, GO, GONR-L and GONR-H are presented in Fig. 3. The original chemical shifts of C-C, C-OH, C-O-C (epoxide or cyclic ether), and O-C=O bonds were positioned at 284.5, 285.7, 286.6, and 288.5 eV, respectively. A tolerance of ±0.3 eV shift from the initial peak position was permitted during the fitting. Shirley algorithm was used to determine background for all regions. The deconvolution of C 1s peaks indicated that oxygen functional groups on GO derivatives were comprised of hydroxyl (C-OH, 285.7 eV), epoxide (O-C-O, 286.6 eV), and carboxyl (O=C-OH, 288.8 eV), however, the majority of these groups in GO, GONR-L,

and GONR-H are hydroxyl/epoxide and few of them are carboxyl groups. A possible explanation for this might be that the carboxyl groups are mainly positioned at the graphene edges while hydroxyl and epoxide are mostly located in the graphene basal plane [48].

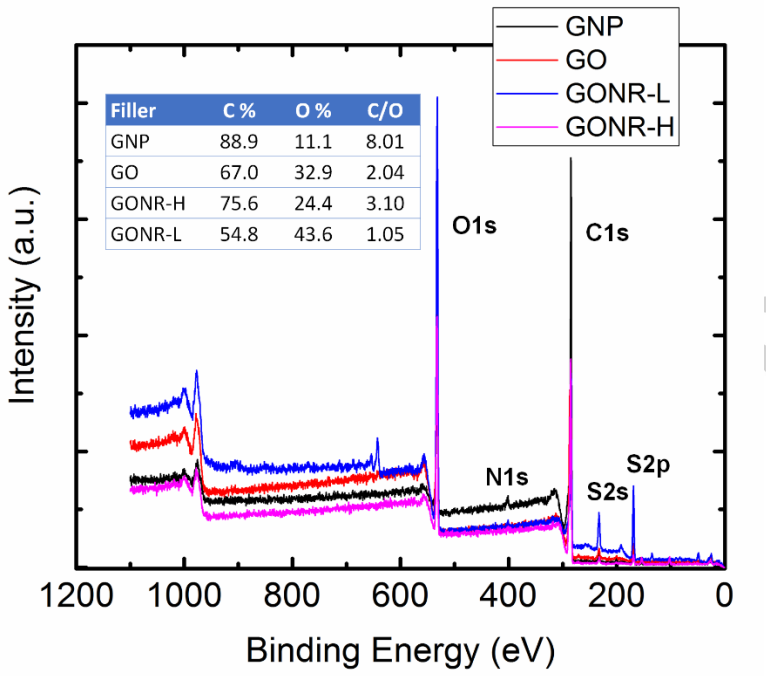

Figure 2: XPS survey spectra of GNP, GO, GONR-L, and GONR-H along with carbon to oxygen ratio (C/O) in these nanofillers

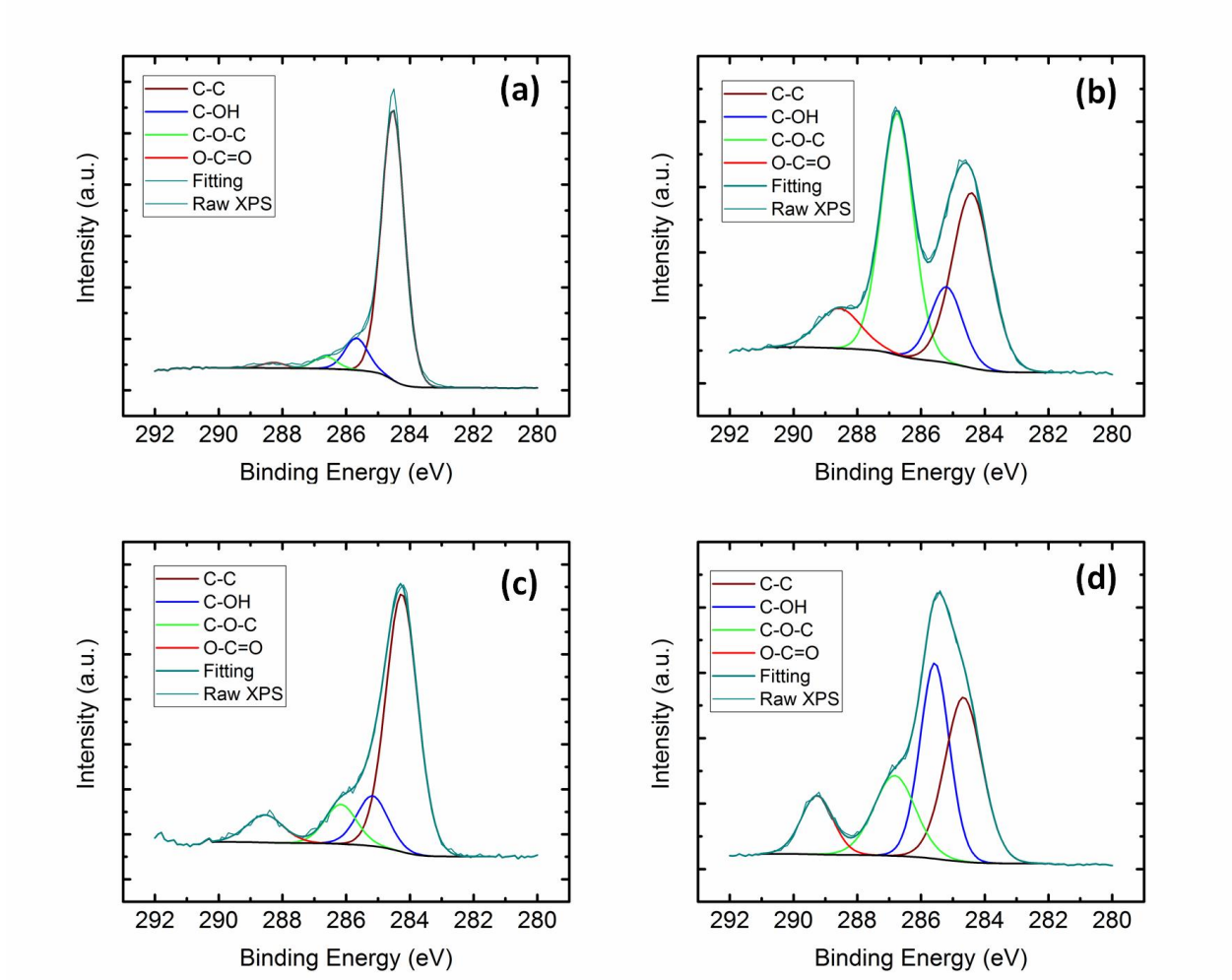

Figure 3: C 1s high-resolution spectra of (a) GNP, (b) GO, (c) GONR-H, and (d) GONR-L

3.3. Surface and cross-section morphology

The internal structure of the pristine PES membrane and GO-based nanocomposite membranes (0.1 wt.% nanofiller) is presented in Fig. 4. As can be observed, all membranes have an asymmetric structure with a dense skin top layer supported by a porous finger-type structure, which is a common internal morphology for NIPS membranes [18,53]. According to Fig. 5, the addition of 0.1 wt.% nanofillers decreased the thickness of membranes with from 120 µm to 100±5 µm. However, the average skin layer thickness increased significantly from 150 nm to 350±50 nm. The addition of GO nanofillers slows down the solvent/nonsolvent exchange rate in the coagulation bath and thus leads to the formation of thinner membranes with thicker skin layer due to the entrapment of more GO nanofillers at the top surface during phase separation [53,54].

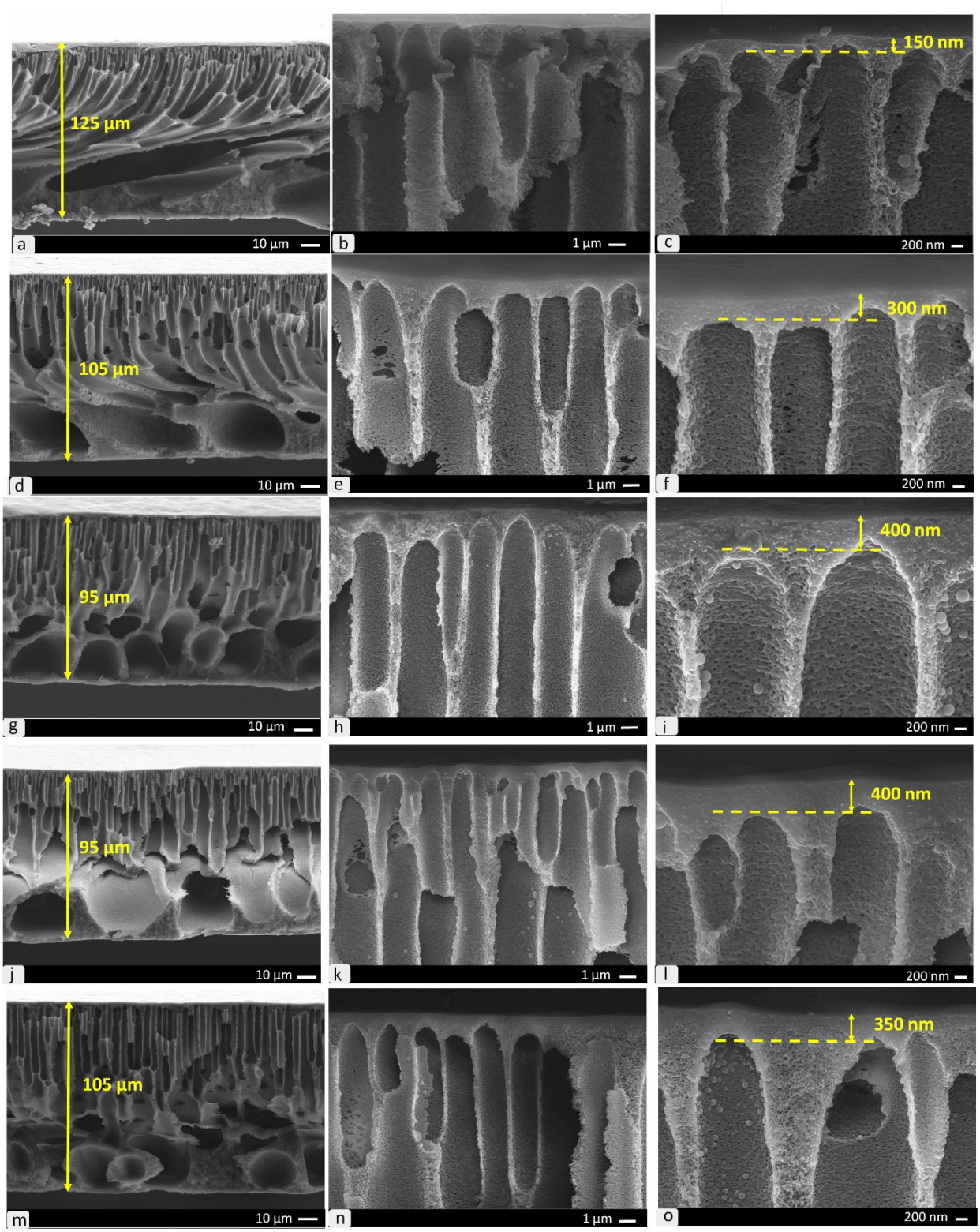

Figure 4: Cross-sectional FESEM images of unmodified PES (a-c) and nanocomposite membranes loaded with 0.1 wt.% of (d-f) GNP, (g-i) GO, (j-l) GONR-L, and (m-o) GONR-H with different magnification

It is worth mentioning that GO nanofillers are hydrophilic additives and tend to enhance thermodynamic instability of casting solution that accelerates the demixing of solvent and nonsolvent. Also, the swelling of the polymer film by hydrophilic nanofillers prior to its solidification allows for more passage of nonsolvent to the casting film during NIPS process and might increase the membrane thickness. However, a significant increase in the viscosity of the casting solution (Fig. S1 in Supporting Information) has countered these effects and increased the skin layer thickness due to a reduction in mutual diffusivities between solvent and nonsolvent.

Fig. 5 shows that the thickness of skin layer increased by increasing the GONR-H loading in the casting solution. The same results were obtained for other types of nanofillers. As can be observed in Fig. 5, the thickness of skin layer increased significantly from 150 nm to 600 nm This finding can also be attributed to an increase in the polymer solution viscosity which reduced the phase inversion rate on the top surface and consequently led to a thicker skin layer.

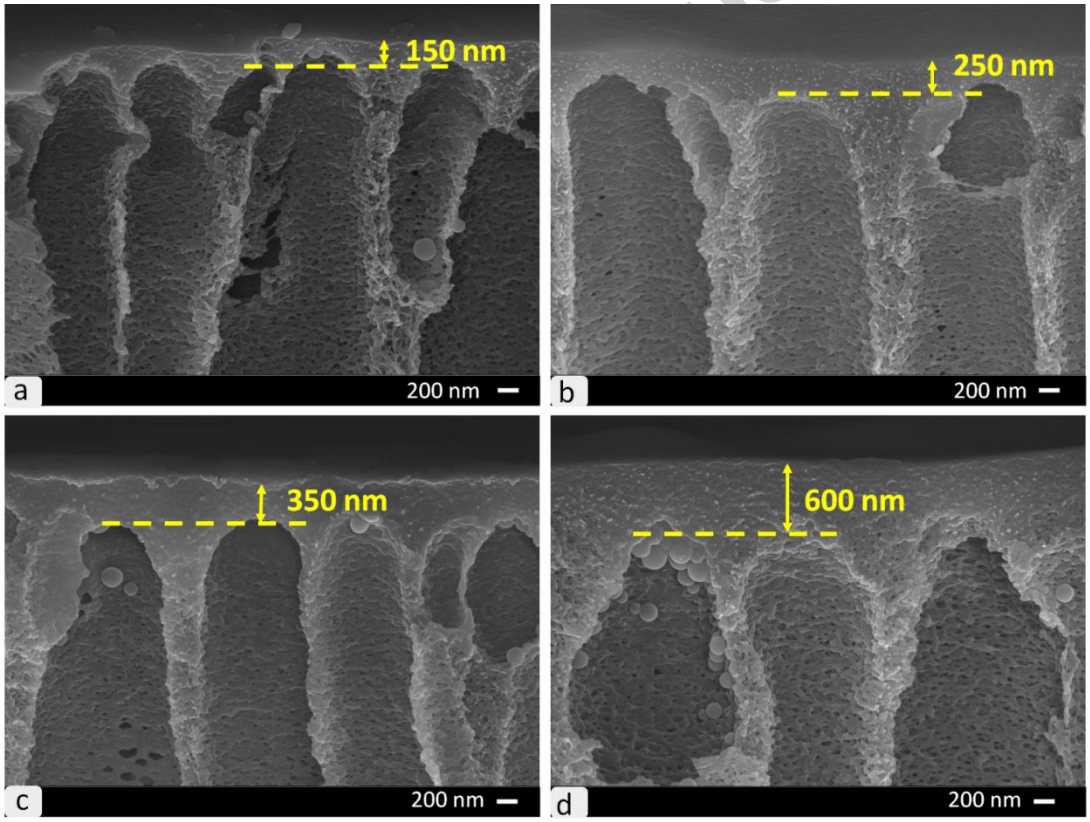

Figure 5: Cross-sectional FESEM images of the skin layer of (a) unmodified PES and nanocomposite membranes containing (b) 0.05 wt.%, (c) 0.1 wt.%, and (d) 0.2 wt.% GONR-H

3.4. Contact Angle measurement results

The hydrophilic property of fabricated membranes can be studied by water contact angle measurement. Surface hydrophilicity is a decisive parameter in determining the antifouling characteristics of NF/UF membranes. Based on sessile drop method, water droplets with a volume of 2 μl were gently placed on the surface of membranes, and the initial contact angle was measured after 3 s. Higher contact angle represents the more hydrophobic surface, and lower contact angle reveals the higher surface energy, as well as, hydrophilic nature of membrane. As presented in Table 4, contact angle decreased with the incorporation of graphene-based nanomaterial into the membrane matrix. The contact angle for the base membrane was 64.6˚. By adding 0.2 wt.% GO, GNR, GONR, and GNP the water contact angle reduced significantly to 43.8˚, 45.6˚, 50.2˚, and 56.9˚, respectively. Since graphene nanomaterials are more hydrophilic than PES, their accumulation on the surface can reduce interface energy. During membrane formation by NIPS method, graphene nanofillers move to the surface of the casting film to be exchanged with water. Most of these nanofillers entrap in the solidified film and thus remain in the polymer matrix. This is justified by the darker color of the top surface as compared to the bottom surface of synthesized membranes. As a result, the contact angle values of all graphene-based nanocomposite membranes were less than the unmodified PES membranes, suggesting that the incorporation of graphene nanofillers leads to the formation of more hydrophilic membranes.

3.5. Membrane surface charge results

Membrane surface charge density can change by the incorporation of nanofillers due to their surface functional groups. The surface charge of synthesized membranes is presented in Table 4. At pH values higher than the isoelectric point (IEP), the sulfonic acid groups in PES polymer become negatively charged ($–SO_3^-$) upon dissociation. By incorporation of GO nanofillers, the membrane surface becomes rich in ionizable functional groups, such as carboxylic and hydroxyl groups, which are responsible for the development of surface charge. At high pH, carboxylic (-COOH) and hydroxyl (-OH) get deprotonated to $–COO^-$ and $–O^-$ negative groups and become the source of electric charge causing the membrane to be negatively charged [55]. The more negative surface charge is proven to reduce fouling by both organic and inorganic materials in the water, which are mostly negatively charged, due to electrostatic repulsion [56,57].

Table 4 Contact angle and zeta potential of unmodified PES and graphene-based nanocomposite membranes

Membranes	Contact Angle	Zeta Potential (mV) at pH 6.5
Unmodified PES	65.2˚ ± 1.8	-20.7 ± 1.6
GNP 0.05 wt.%	63.3˚ ± 0.7	-22.2 ± 0.7
GNP 0.1 wt.%	61.6˚ ± 1.0	-22.5 ± 0.8
GNP 0.2 wt.%	56.9˚ ± 1.1	-23.1 ± 1.0
GO 0.05 wt.%	58.6˚ ± 0.6	-25.1 ± 1.9
GO 0.1 wt.%	51.1˚ ± 0.9	-28.0 ± 0.6
GO 0.2 wt.%	43.8˚ ± 1.0	-29.7 ± 2.3
GONR-L 0.05 wt.%	57.5˚ ± 1.0	-24.2 ± 1.4
GONR-L 0.1 wt.%	51.8˚ ± 1.1	-26.8 ± 1.6
GONR-L 0.2 wt.%	45.6˚ ± 0.4	-28.6 ± 2.3
GONR-H 0.05 wt.%	59.2˚ ± 1.2	-22.7 ± 1.2
GONR-H 0.1 wt.%	56.0˚ ± 0.9	-24.4 ± 0.8
GONR-H 0.2 wt.%	50.2˚ ± 1.6	-23.2 ± 1.4

3.6. Permeability of membranes

The pure water flux of unmodified PES membrane and nanocomposite membranes with 0.1 wt.% loading of nanofillers, as a function transmembrane pressure, is shown in Fig. 6a. The slopes in this figure indicate the hydraulic permeability of the membranes. As can be seen, incorporating 0.1 wt.% of all graphene nanofillers has led to the higher water permeability than pristine PES membrane. This improvement can be attributed to the improved surface hydrophilicity (Table 4) by the incorporation of more hydrophilic hydroxyl groups to the surface [57]. The nanocomposite membrane prepared by GONR-L was found to provide the maximum hydraulic permeability of 1.30 LMH/psi.

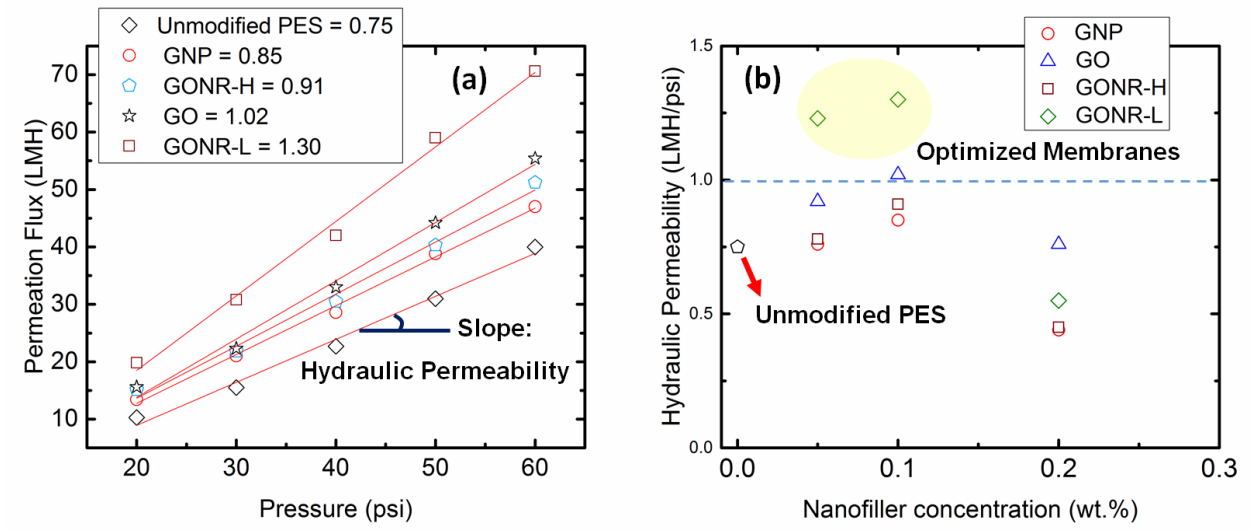

Figure 6: (a) Pure water flux vs pressure for unmodified PES membrane and nanocomposite membranes prepared by 0.1wt. % GO derivative nanofillers (the slope represents hydraulic permeability of membranes), (b) hydraulic permeability of membranes as a function of nanofillers loading in membrane

The effect of nanofillers concentration on the hydraulic permeability of membranes is shown in Fig. 6b. Hydraulic permeability data in this figure are extracted from flux vs. pressure graphs as presented in Figure S2 in Supporting Information. As can be seen in Figure 6b, increasing the concentration of nanofillers up to 0.1 wt.% increased the water permeability, however, further increase up to 0.2 wt.% decreased the water permeation, significantly, to even less than that of unmodified PES membrane. Theoretically, the porosity of phase inversion membranes is influenced by a trade-off between thermodynamic enhancement and kinetic hindrance of the casting solution [58]. The addition of hydrophilic nanofillers to polymer solution induces thermodynamic instability. The thermodynamic variation enhances the demixing rate of solvent and non-solvent in the casting solution, thus leading to the formation of more porous structures, whereas the rheological variation induces the opposite trend. A significant increase in the viscosity of casting solution (Figure S1 in Supporting Information) by the addition 0.2 wt.% nanofillers has led to the delayed demixing of solvent and non-solvent and thus formation of denser structures due to the dominant role of the kinetic hindrance. This implies the presence of an optimum loading of nanofillers for improving the water flux.

It is worth mentioning that the addition of higher concentration of nanofillers not only affects the overall porosity of the membrane but also changes the thickness and morphology of skin layer

which is mainly responsible for the permeation properties of membranes. In the present study, another reason for the significant decrease in the water flux by the addition of 0.2 wt.% nanofillers can be due to the notable increase in the thickness of skin layer (FESEM images in Fig. 4).

3.7. Porosity and mean pore radius of membrane

Fig. 7 shows overall porosity of nanocomposite membranes. By the addition of a low quantity of graphene-based nanofillers up to 0.1 wt.%, the overall porosity is initially increased, then reduced by further addition of the nanofillers up to 0.2 wt.%. This behavior is also reported by other researchers [46,60,61]. Incorporation of hydrophilic nanofillers at low content into the polymer matrix could enhance amorphous nature of membranes; together with the rapid exchange of DMAc and water in NIPS process, the overall porosity of nanocomposite membrane increases [52]. This trend is consistent with the water flux results that showed a convex profile with increasing nanofillers. In addition, incorporation of hydrophilic nanofillers increases the thermodynamic instability of casting solution in the coagulation bath which leads to an accelerated solvent and nonsolvent exchange and large pore formation [59]. In the case of high nanofillers loading, the mean pore size decreased (Fig. 8) because of an apparent increase in the viscosity of the polymer solution. As mentioned earlier, increased viscosity causes a delay in demixing and thus suppresses the formation of large pore size.

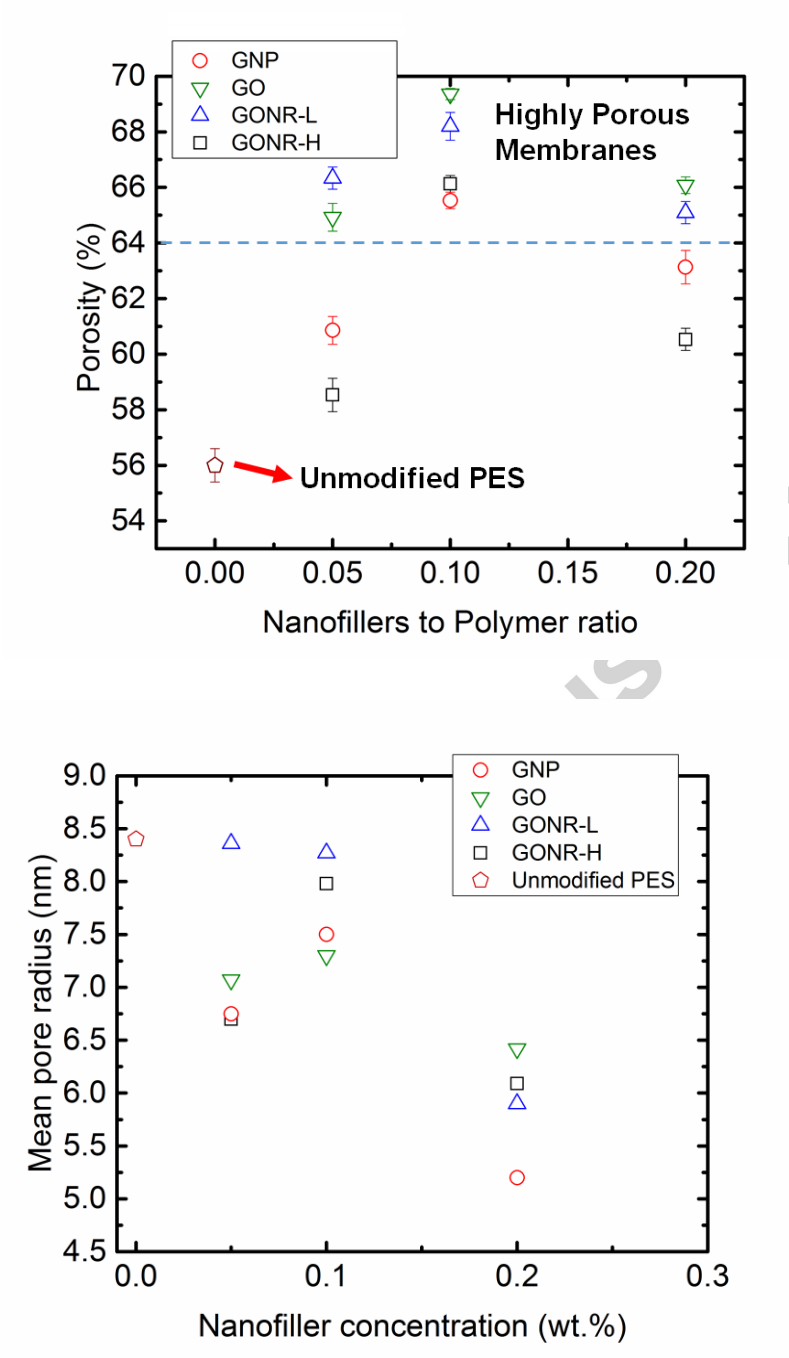

Figure 7: a) Membranes porosity in the different loading of graphene-based nanofillers. b) Mean pore radius of the membrane as a function of nanofiller concentration

Fig. 7b shows that the addition of nanofillers decreased the pore size of membranes. By increasing the nanofiller loading to 0.2 wt.% the mean pore size of membrane reduced significantly from 8.4 nm for pristine PES membrane to 6.2, 6.0, 5.8, and 5.2 nm for GO, GONR-H, GONR-L, and GNP, respectively.

3.8. Separation performance of membranes

The separation performance of synthesized membranes was evaluated by filtration of PEG solution and WLS inlet water. 250 mg/L solutions of PEG with a nominal average molar mass of 35,000 g/mol with the mean molecular diameter [62] of 8.92 nm was filtered, and concentration of PEG in permeate was measured using TOC analyzer. The rejection results are presented in Table 5. WLS inlet filtration results show superior performance of nanocomposite membranes for the removal of organic matter from oil sands produced water. The rejection increased from 43% to more than 50% for all GO-based nanocomposite membranes. Based on the data presented in Fig. 4 and Table 5, the addition of 0.1 wt.% GONR-L has maximized both water flux (70 LMH at 60 psi) and TOC rejection (59%). PEG rejection results confirm that the molecular weight cut-off (MWCO) of modified membranes is about 35 kDa [59].

Table 5: WLS inlet and PEG rejection by graphene-based nanocomposite membranes

Membranes	WLS inlet Rejection (%)	PEG (Mw=35000 g/mol) Rejection (%)
Unmodified PES	43	86
GNP 0.05 wt.%	47	88
GNP 0.1 wt.%	49	90
GNP 0.2 wt.%	51	90
GO 0.05 wt.%	57	92
GO 0.1 wt.%	58	97
GO 0.2 wt.%	55	96
GONR-L 0.05 wt.%	55	88
GONR-L 0.1 wt.%	59	92
GONR-L 0.2 wt.%	57	94
GONR-H 0.05 wt.%	50	90
GONR-H 0.1 wt.%	50	91
GONR-H 0.2 wt.%	52	91

3.9. Fouling characteristics of membranes

The fouling behavior of the graphene-based nanocomposite membranes and unmodified PES membrane during filtration of WLS inlet water is presented in the Fig. 8. Experiments were conducted at the same initial flux to investigate the effect of induced surface properties by graphene nanofillers on flux decline. Constant initial flux ensures a constant permeation drag for all experiments and thus fouling intensity can be attributed to surface properties like hydrophilicity and surface charge [57]. Also, all membranes were compacted at higher pressure before filtration test to make sure that the flux decline over time is just due to the fouling phenomenon [29].

As can be observed in Fig. 8, the flux decline in graphene-based nanocomposite membranes was less than unmodified PES membranes. After 160 min filtration, GONR-L membrane showed 30% more water flux than pristine PES membrane (16 LMH compared to 11 LMH) that demonstrate its antifouling property for the filtration of WLS inlet water. This result can be attributed to higher hydrophilicity and more negatively charged surface of GONR-L (Table 4) that mitigated fouling through electrostatic repulsion and reduced hydrophobic interaction mechanisms.

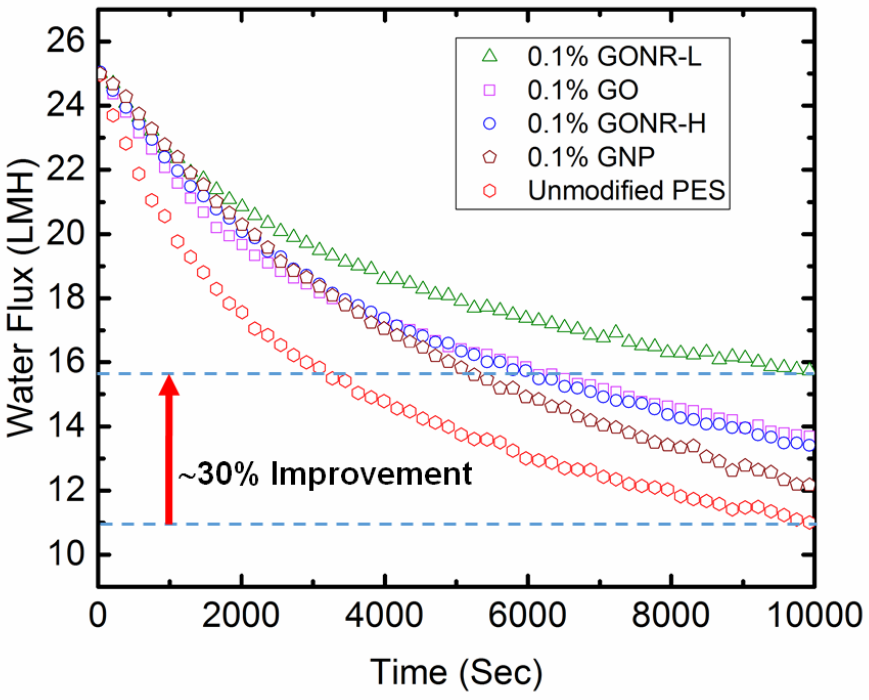

Figure 8: Flux vs. time of nanocomposite membranes and unmodified PES membrane due to fouling by WLS inlet water, compared at the same initial flux

Fouling behavior of a membrane is controlled by several parameters such as membrane surface properties (e.g., zeta potential and hydrophilicity), feed solution chemistry (e.g., ionic strength, and pH) and hydrodynamic of membrane modules [63,64]. In this research to investigate membrane surface properties, the latter two parameters and temperature were kept similar during experiments. It is generally accepted that the membrane with higher hydrophilicity and more negative surface charge are more resistant to fouling owing to fewer interactions among the polar groups on the membrane surface and the functional groups of the dissolved organic compounds in the feed. A possible explanation is that the formation of hydrogen bonding among the surface hydrophilic groups and water molecules forms a water layer on membrane surface that could impede membrane-foulant attachment [58,65]. Also, organic matter in the fluids tested are mostly hydrophobic [66] and, therefore are less inclined to attach to a hydrophilic surface due to the smaller hydrophobic interaction between fouling material and membrane surface. The combination of the hydrophilic surface of graphene-based nanocomposite membranes along with their high surface potential made them less inclined to fouling by suspended organic matter, which may be beneficial for oil sands produced water treatment.

Water flux recovery ratio (FRR), total flux decline ratio (DR_t), irreversible fouling ratio (DR_{ir}), and reversible fouling ratio (DR_r) for the base and 0.1 wt.% graphene-based nanofillers/PES membranes are depicted in Fig. 9. All membranes showed flux decline during filtration of WLS inlet water for 1 hour which was likely due to deposition of organic and inorganic materials on the surface of membranes. However, the irreversible flux reduction due to strong adsorption of foulants on the surface and pores of the membranes was decreased for graphene-based nanocomposite membranes (GO: 9.3%, GONR-L: 10%, GNP: 19%, GONR-H: 19%) in comparisons with unmodified PES membrane (24%). The flux decline of graphene-based nanocomposite membrane was 14% less than the unmodified PES membrane at the same condition. Also, GO/PES and GONR-L/PES membranes indicated 14% more flux recovery ratio than the unmodified PES membrane, implying an enhancement in antifouling characteristics of the base membrane by the incorporation of GO and GONR-L nanofillers. However, FRR enhanced only 4% after the addition of GNP and GONR-H which might be due to the lack of oxygen functional groups on GNP surface.

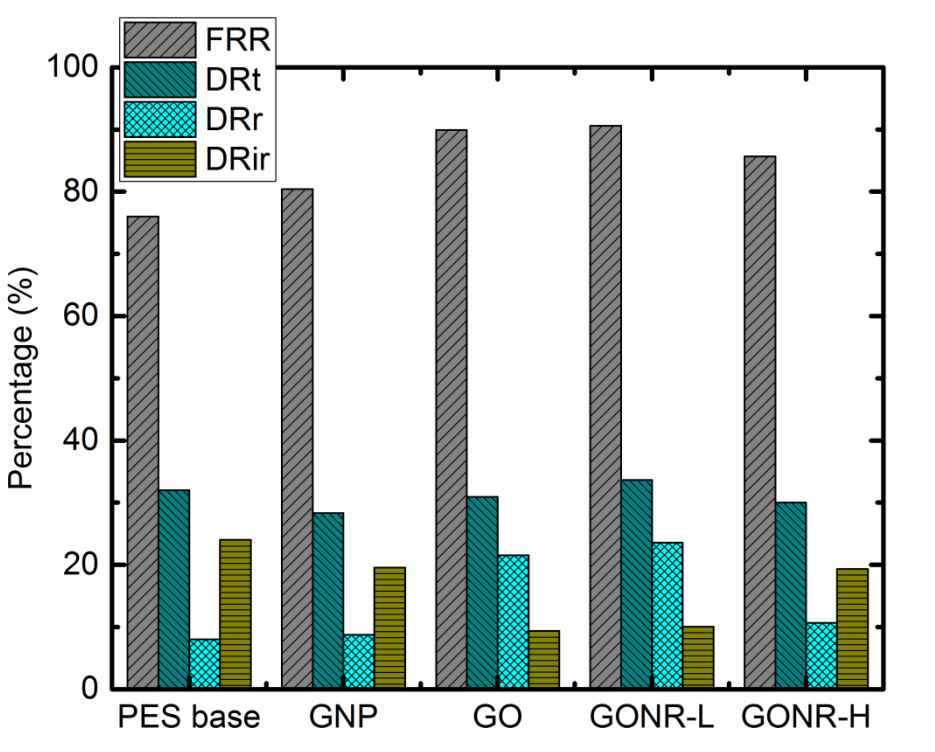

Figure 9: Comparison of the fouling characteristics of PES/ Graphene-based nanofillers membranes and unmodified membrane. DRt is total flux decline ratio, DRr is reversible flux decline, DRir is irreversible flux decline ratio, and FRR is flux recovery ratio.

4. Conclusions

In this study, graphene oxide derivatives with different shapes and oxidation states were incorporated into a polymeric membrane matrix via NIPS technique. The surface properties of the fabricated membranes have significantly changed in terms of hydrophilicity and surface charge. The contact angle and streaming potential measurements demonstrated the fabrication of more hydrophilic and negatively charged PES/GO nanocomposite membranes. All graphene-based nanocomposite membranes showed better water flux and rejection of organic matter than unmodified PES membrane. The addition of graphene nanofillers, up to 0.1 wt.%, first enhanced the water flux due to an increase in overall porosity and hydrophilicity of the membranes, then further increase of nanofillers loading decreased the flux more likely due to the formation of a thicker skin layer. The optimum loading to improve both water flux and rejection of organic matter was found to be 0.1 wt.%. The graphene-based nanocomposite membranes were found to have an MWCO of ~35 kDa and removed 50% of dissolved organic matter from SAGD produced water. Fouling propensity of membranes was tested with SAGD WLS inlet water. The results show that

by the addition of graphene nanofillers the fouling tendency of the membranes has hindered due to improved surface properties. GONR-L at its optimum loading (0.1 wt.%) has provided the maximum water flux (70 LMH at 60 psi), TOC rejection (59%) and antifouling properties (30% improvement compared to pristine PES membrane). The flux recovery ratio (FRR) experiments have confirmed significant improvement in the antifouling property of PES/GO nanocomposite membranes.

Acknowledgment

The authors would like to thank Apoorv Sinha (Carbon Upcycling Technologies, Calgary, Canada) for synthesizing and supplying GO nanosheets, and Matthew Martz (University of Waterloo) for assisting in the synthesis of GONR-H and GONR-L. The authors would also thank Dr. Payman Esmaeili at Imperial Oil who connected the two groups at U of Alberta and U of Waterloo. Financial support for this work through the Natural Sciences and Engineering Research Council of Canada (NSERC), Natural Resources Canada (NRCan), Suncor Energy, Devon Canada, ConocoPhillips, and Water Institute at the University of Waterloo is gratefully acknowledged.

Supporting Information

The Supporting Information file includes (1) viscosity of casting solution as a function of GO content at different shear rates; (2) water flux vs. pressure for different concentration of GNP, GO, GONR-L, and GONR-H; (3) magnified C1s and O1s XPS survey spectra of GNP, GO, GONR-L, and GONR-H nanofillers.

References:

[1] M. Hu, B. Mi, Enabling graphene oxide nanosheets as water separation membranes, Environ. Sci. Technol. 47 (2013) 3715–3723. doi:10.1021/es400571g.

[2] L.Y. Ng, A.W. Mohammad, C.P. Leo, N. Hilal, Polymeric membranes incorporated with metal/metal oxide nanoparticles: A comprehensive review, Desalination. 308 (2013) 15–33. doi:10.1016/j.desal.2010.11.033.

[3] R. Rezaee, S. Nasseri, A.H. Mahvi, R. Nabizadeh, S.A. Mousavi, A. Rashidi, A. Jafari, S. Nazmara, ENVIRONMENTAL HEALTH Fabrication and characterization of a polysulfone-graphene oxide nanocomposite membrane for arsenate rejection from water, J. Environ. Heal. Sci. Eng. (2015) 1–11. doi:10.1186/s40201-015-0217-8.

[4] S. Zinadini, A.A. Zinatizadeh, M. Rahimi, V. Vatanpour, H. Zangeneh, Preparation of a novel antifouling mixed matrix PES membrane by embedding graphene oxide nanoplates, J. Memb. Sci. 453 (2014) 292–301. doi:10.1016/j.memsci.2013.10.070.

[5] X. Shi, G. Tal, N.P. Hankins, V. Gitis, Journal of Water Process Engineering Fouling and cleaning of ultrafiltration membranes : A review, J. Water Process Eng. 1 (2014) 121–138. doi:10.1016/j.jwpe.2014.04.003.

[6] A. Seidel, M. Elimelech, Coupling between chemical and physical interactions in natural organic matter (NOM) fouling of nanofiltration membranes : implications for fouling control, J. Memb. Sci. 203 (2002) 245–255.

[7] S. Hong, M. Elimelech, Chemical and physical aspects of natural organic matter (NOM) fouling of nanofiltration membranes, J. Memb. Sci. 132 (1997) 159–181. doi:10.1016/S0376-7388(97)00060-4.

[8] K.C. Khulbe, C. Feng, T. Matsuura, The art of surface modification of synthetic polymeric membranes, J. Appl. Polym. Sci. 115 (2009) 855–895. doi:10.1002/app.

[9] D. Rana, T. Matsuura, Surface modifications for antifouling membranes, Chem. Rev. 110 (2010) 2448–2471. doi:10.1021/cr800208y.

[10] R. Zhang, Y. Liu, M. He, Y. Su, X. Zhao, M. Elimelech, Z. Jiang, Antifouling membranes for sustainable water purification: strategies and mechanisms., Chem. Soc. Rev. 45 (2016) 5888–5924. doi:10.1039/c5cs00579e.

[11] J. Yin, B. Deng, Polymer-matrix nanocomposite membranes for water treatment, J. Memb. Sci. 479 (2014) 256–275. doi:10.1016/j.memsci.2014.11.019.

[12] D.J. Miller, D.R. Dreyer, C.W. Bielawski, D.R. Paul, B.D. Freeman, Surface Modification of Water Purification Membranes, Angew.Chem.Int. 56 (2017) 4662–4711. doi:10.1002/anie.201601509.

[13] B. Khorshidi, B. Soltannia, T. Thundat, M. Sadrzadeh, Synthesis of thin film composite polyamide membranes: Effect of monohydric and polyhydric alcohol additives in aqueous solution, J. Memb. Sci. 523 (2017) 336–345. doi:10.1016/j.memsci.2016.09.062.

[14] O. Burtovyy, V. Klep, T. Turel, Y. Gowayed, I. Luzinov, Polymeric membranes: Surface modification by “grafting to” method and fabrication of multilayered assemblies, ACS Symp. Ser. 1016 (2009) 289–305. doi:10.1021/bk-2009-1016.ch022.

[15] J.M. Grace, L.J. Gerenser, Plasma Treatment of Polymers, J. Dispers. Sci. Technol. 24 (2003) 305–341. doi:10.1081/DIS-120021793.

[16] E.F. Castro Vidaurre, C. a. Achete, F. Gallo, D. Garcia, R. Simão, a. C. Habert, Surface Modification of Polymeric Materials by Plasma Treatment, Mater. Res. 5 (2002) 37–41. doi:10.1590/S1516-14392002000100006.

[17] Z. Wang, H. Yu, J. Xia, F. Zhang, F. Li, Y. Xia, Y. Li, Novel GO-blended PVDF ultrafiltration membranes, Desalination. 299 (2012) 50–54. doi:10.1016/j.desal.2012.05.015.

[18] M. Amirilargani, M. Sadrzadeh, T. Mohammadi, Synthesis and characterization of polyethersulfone membranes, J. Polym. Res. 17 (2009) 363–377. doi:10.1007/s10965-009-9323-6.

[19] Y. Zhang, P. Liu, Polysulfone(PSF) composite membrane with micro-reaction locations (MRLs) made by doping sulfated TiO2 deposited on SiO2 nanotubes (STSNs) for cleaning wastewater, J. Memb. Sci. 493 (2015) 275–284. doi:10.1016/j.memsci.2015.06.011.

[20] M.L. Luo, J.Q. Zhao, W. Tang, C.S. Pu, Hydrophilic modification of poly(ether sulfone) ultrafiltration membrane surface by self-assembly of TiO2 nanoparticles, Appl. Surf. Sci. 249 (2005) 76–84. doi:10.1016/j.apsusc.2004.11.054.

[21] Y. Zhang, L. Wang, Y. Xu, Effect of doping porous ZrO2 solid superacid shell/void/TiO2 core nanoparticles (ZVT) on properties of polyvinylidene fluoride (PVDF) membranes, Desalination. 358 (2015) 84–93. doi:10.1016/j.desal.2014.12.022.

[22] Y. Zhang, P. Liu, Preparation of porous ZrO2 solid superacid shell/void/TiO2 core particles and effect of doping them on PVDF membranes properties, Chem. Eng. Sci. 135 (2015) 67–75. doi:10.1016/j.ces.2015.06.037.

[23] A. Bottino, G. Capannelli, A. Comite, Preparation and characterization of novel porous PVDF-Zr02 composite membranes, 146 (2002) 35–40.

[24] Y. Zhang, L. Wang, Y. Xu, ZrO2 solid superacid porous shell/void/TiO2 core particles (ZVT)/polyvinylidene fluoride (PVDF) composite membranes with anti-fouling performance for sewage treatment, Chem. Eng. J. 260 (2015) 258–268. doi:10.1016/j.cej.2014.08.083.

[25] L. Yan, Y.S. Li, C.B. Xiang, S. Xianda, Effect of nano-sized Al2O3-particle addition on PVDF ultrafiltration membrane performance, J. Memb. Sci. 276 (2006) 162–167. doi:10.1016/j.jsb.2006.03.024.

[26] Y. Zhang, F. Liu, Y. Lu, L. Zhao, L. Song, Investigation of phosphorylated TiO2–SiO2 particles/polysulfone composite membrane for wastewater treatment, Desalination. 324 (2013) 118–126. doi:10.1016/j.desal.2013.06.007.

[27] J. Shen, H. Ruan, L. Wu, C. Gao, Preparation and characterization of PES – SiO 2 organic – inorganic composite ultrafiltration membrane for raw water pretreatment, 168 (2011) 1272–1278. doi:10.1016/j.cej.2011.02.039.

[28] N. Ghaemi, S.S. Madaeni, P. Daraei, H. Rajabi, S. Zinadini, A. Alizadeh, R. Heydari, M. Beygzadeh, S. Ghouzivand, Polyethersulfone membrane enhanced with iron oxide nanoparticles for copper removal from water: Application of new functionalized Fe3O4 nanoparticles, Chem. Eng. J. 263 (2015) 101–112. doi:10.1016/j.cej.2014.10.103.

[29] B. Khorshidi, J. Hajinasiri, G. Ma, S. Bhattacharjee, M. Sadrzadeh, Thermally resistant and electrically conductive PES/ITO nanocomposite membrane, J. Memb. Sci. 500 (2016) 151–160. doi:10.1016/j.memsci.2015.11.015.

[30] V. Moghimifar, A.E. Livari, A. Raisi, A. Aroujalian, RSC Advances Enhancing the antifouling property of polyethersulfone ultra fi ltration membranes using NaX zeolite and

titanium oxide nanoparticles, RSC Adv. 5 (2015) 55964–55976. doi:10.1039/C5RA06986F.

[31] E. Celik, H. Park, H. Choi, H. Choi, Carbon nanotube blended polyethersulfone membranes for fouling control in water treatment, Water Res. 45 (2011) 274–282. doi:10.1016/j.watres.2010.07.060.

[32] L. Wang, X. Song, T. Wang, S. Wang, Z. Wang, C. Gao, Applied Surface Science Fabrication and characterization of polyethersulfone / carbon nanotubes (PES / CNTs) based mixed matrix membranes (MMMs) for nanofiltration application, Appl. Surf. Sci. 330 (2015) 118–125. doi:10.1016/j.apsusc.2014.12.183.

[33] D. Zhang, A. Karkooti, L. Liu, M. Sadrzadeh, T. Thundat, Y. Liu, R. Narain, Fabrication of antifouling and antibacterial polyethersulfone (PES)/cellulose nanocrystals (CNC) nanocomposite membranes, J. Memb. Sci. 549 (2017) 350–356. doi:10.1016/j.memsci.2017.12.034.

[34] B.M. Ganesh, A.M. Isloor, A.F. Ismail, Enhanced hydrophilicity and salt rejection study of graphene oxide-polysulfone mixed matrix membrane, Desalination. 313 (2013) 199–207. doi:10.1016/j.desal.2012.11.037.

[35] G. Mittal, V. Dhand, K.Y. Rhee, S.-J. Park, W.R. Lee, A review on carbon nanotubes and graphene as fillers in reinforced polymer nanocomposites, J. Ind. Eng. Chem. 21 (2015) 11–25. doi:10.1016/j.jiec.2014.03.022.

[36] H. Kim, A.A. Abdala, C.W. MacOsko, Graphene/polymer nanocomposites, Macromolecules. 43 (2010) 6515–6530. doi:10.1021/ma100572e.

[37] K. Hu, D.D. Kulkarni, I. Choi, V. V. Tsukruk, Graphene-polymer nanocomposites for structural and functional applications, Prog. Polym. Sci. 39 (2014) 1934–1972. doi:10.1016/j.progpolymsci.2014.03.001.

[38] T. Kuilla, S. Bhadra, D. Yao, N.H. Kim, S. Bose, J.H. Lee, Recent advances in graphene based polymer composites, Prog. Polym. Sci. 35 (2010) 1350–1375. doi:10.1016/j.progpolymsci.2010.07.005.

[39] A. Fonseca, S. Nejati, M. Elimelech, Antimicrobial properties of graphene oxide nanosheets: Why size matters, ACS Nano. 9 (2015) 7226–7236. doi:10.1021/ascnano.5b02067.

[40] O.C. Compton, S.T. Nguyen, Graphene oxide, highly reduced graphene oxide, and graphene: Versatile building blocks for carbon-based materials, Small. 6 (2010) 711–723. doi:10.1002/smll.200901934.

[41] L. Yu, Y. Zhang, B. Zhang, J. Liu, H. Zhang, C. Song, Preparation and characterization of HPEI-GO/PES ultrafiltration membrane with antifouling and antibacterial properties, J. Memb. Sci. 447 (2013) 452–462. doi:10.1016/j.memsci.2013.07.042.

[42] J. Lee, H.R. Chae, Y.J. Won, K. Lee, C.H. Lee, H.H. Lee, I.C. Kim, J. min Lee, Graphene oxide nanoplatelets composite membrane with hydrophilic and antifouling properties for wastewater treatment, J. Memb. Sci. 448 (2013) 223–230. doi:10.1016/j.memsci.2013.08.017.

[43] J.L. Yuanyuan Zhao, Jiaqi Lu, Xuyang Liu, Yudan Wang, Jiuyang Lin, Na Peng, F. Zhao, Performance enhancement of polyvinyl chloride ultrafiltration membrane modified with graphene oxide, J. Colloid Interface Sci. 480 (2016) 1–8. doi:10.1016/j.jcis.2016.06.075.

[44] H. Wu, B. Tang, P. Wu, Development of novel SiO2-GO nanohybrid/polysulfone membrane with enhanced performance, J. Memb. Sci. 451 (2014) 94–102. doi:10.1016/j.memsci.2013.09.018.

[45] M.Y. Lim, Y.S. Choi, J. Kim, K. Kim, H. Shin, J.J. Kim, D.M. Shin, J.C. Lee, Cross-linked graphene oxide membrane having high ion selectivity and antibacterial activity prepared using tannic acid-functionalized graphene oxide and polyethyleneimine, J. Memb. Sci. 521 (2017) 1–9. doi:10.1016/j.memsci.2016.08.067.

[46] Z. Xu, J. Zhang, M. Shan, Y. Li, B. Li, J. Niu, B. Zhou, X. Qian, Organosilane-functionalized graphene oxide for enhanced antifouling and mechanical properties of polyvinylidene fluoride ultrafiltration membranes, J. Memb. Sci. 458 (2014) 1–13. doi:10.1016/j.memsci.2014.01.050.

[47] S. Sadeghi, A. Zehtab Yazdi, U. Sundararaj, Controlling Short-Range Interactions by Tuning Surface Chemistry in HDPE/Graphene Nanoribbon Nanocomposites, J. Phys. Chem. B. 119 (2015) 11867–11878. doi:10.1021/acs.jpcb.5b03558.

[48] A.Z. Yazdi, K. Chizari, A.S. Jalilov, J. Tour, U. Sundararaj, A. Zehtab Yazdi, K. Chizari, A.S. Jalilov, J. Tour, U. Sundararaj, Helical and Dendritic Unzipping of Carbon Nanotubes: A Route to Nitrogen-Doped Graphene Nanoribbons, ACS Nano. (2015) 5833–5845. doi:10.1021/acsnano.5b02197.

[49] A. Zehtab Yazdi, H. Fei, R. Ye, G. Wang, J. Tour, U. Sundararaj, Boron/nitrogen co-doped helically unzipped multiwalled carbon nanotubes as efficient electrocatalyst for oxygen reduction, ACS Appl. Mater. Interfaces. 7 (2015) 7786–7794. doi:10.1021/acsami.5b01067.

[50] A.L. Higginbotham, D. V Kosynkin, A. Sinitskii, Z. Sun, J.M. Tour, Lower-Defect Graphene Oxide Nanotubes, 4 (2010) 2059–2069.

[51] D. V. Kosynkin, A.L. Higginbotham, A. Sinitskii, J.R. Lomeda, A. Dimiev, B.K. Price, J.M. Tour, Longitudinal unzipping of carbon nanotubes to form graphene nanoribbons, Nature. 458 (2009) 872–876. doi:10.1038/nature07872.

[52] V. Vatanpour, S.S. Madaeni, R. Moradian, S. Zinadini, B. Astinchap, Novel antibifouling nanofiltration polyethersulfone membrane fabricated from embedding TiO2 coated multiwalled carbon nanotubes, Sep. Purif. Technol. 90 (2012) 69–82. doi:10.1016/j.seppur.2012.02.014.

[53] E. Saljoughi, M. Sadrzadeh, T. Mohammadi, Effect of preparation variables on morphology and pure water permeation flux through asymmetric cellulose acetate membranes, J. Memb. Sci. 326 (2009) 627–634. http://www.sciencedirect.com/science/article/B6TGK-4TVHSM7-9/2/c732bd3b4ae4533c69aa261ea23c2a1c.

[54] V.R.S.S. Mokkapati, D.Y. Koseoglu-Imer, N. Yilmaz-Deveci, I. Mijakovic, I. Koyuncu,

Membrane properties and anti-bacterial/anti-biofouling activity of polysulfone–graphene oxide composite membranes phase inversed in graphene oxide non-solvent, RSC Adv. 7 (2017) 4378–4386. doi:10.1039/C6RA25015G.

[55] K.C. Khulbe, C. Feng, T. Matsuura, Synthetic Polymeric Membranes, Characterization by Atomic Force Microscopy, Springer, 2008. doi:10.1007/978-3-540-73994-4.

[56] D. V. Bavykin, E. V. Milsom, F. Marken, D.H. Kim, D.H. Marsh, D.J. Riley, F.C. Walsh, K.H. El-Abiary, A.A. Lapkin, A novel cation-binding TiO2 nanotube substrate for electro-catalysis and bioelectro-catalysis, Electrochem. Commun. 7 (2005) 1050–1058.

[57] M. Hayatbakhsh, M. Sadrzadeh, D. Pernitsky, S. Bhattacharjee, J. Hajinasiri, Treatment of an in situ oil sands produced water by polymeric membranes, Desalin. Water Treat. 57 (2016) 14869–14887.

[58] X. Zhao, J. Ma, Z. Wang, G. Wen, J. Jiang, F. Shi, L. Sheng, Hyperbranched-polymer functionalized multi-walled carbon nanotubes for poly (vinylidene fluoride) membranes: From dispersion to blended fouling-control membrane, Desalination. 303 (2012) 29–38. doi:10.1016/j.desal.2012.07.009.

[59] M. Sadrzadeh, S. Bhattacharjee, Rational design of phase inversion membranes by tailoring thermodynamics and kinetics of casting solution using polymer additives, J. Memb. Sci. 441 (2013) 31–44. doi:10.1016/j.memsci.2013.04.009.

[60] V. Vatanpour, S.S. Madaeni, L. Rajabi, S. Zinadini, A.A. Derakhshan, Boehmite nanoparticles as a new nanofiller for preparation of antifouling mixed matrix membranes, J. Memb. Sci. 401–402 (2012) 132–143. doi:10.1016/j.memsci.2012.01.040.

[61] P. Wang, J. Ma, Z. Wang, F. Shi, Q. Liu, Enhanced separation performance of PVDF/PVP-g-MMT nanocomposite ultrafiltration membrane based on the NVP-grafted polymerization modification of montmorillonite (MMT), Langmuir. 28 (2012) 4776–4786. doi:10.1021/la203494z.

[62] S. Lentsch, P. Aimar, J.L. Orozco, Separation albumin-PEG: Transmission of PEG through ultrafiltration membranes, Biotechnol. Bioeng. 41 (1993) 1039–1047. doi:10.1002/bit.260411106.

[63] V. Kochkodan, D.J. Johnson, N. Hilal, Polymeric membranes: Surface modification for minimizing (bio)colloidal fouling, Adv. Colloid Interface Sci. 206 (2014) 116–140. doi:10.1016/j.cis.2013.05.005.

[64] V. Kochkodan, Reduction of Membrane Fouling by Polymer Surface Modification, in: Membr. Modif. Technol. Appl., CRC Press, 2012: pp. 41–76. doi:doi:10.1201/b12160-4.

[65] C. Bellona, J.E. Drewes, The role of membrane surface charge and solute physico-chemical properties in the rejection of organic acids by NF membranes, J. Memb. Sci. 249 (2005) 227–234. doi:10.1016/j.memsci.2004.09.041.

[66] A. Maiti, M. Sadrzadeh, S. Guha Thakurta, D.J. Pernitsky, S. Bhattacharjee, Characterization of boiler blowdown water from steam-assisted gravity drainage and silica–organic coprecipitation during acidification and ultrafiltration, Energy & Fuels. 26 (2012) 5604–5612. doi:10.1021/ef300865e.

Highlights:

1. Graphene oxide nanoribbons were used for the first time to develop nanocomposite membranes
2. The effect of shape and oxidation state of nanofillers on membrane properties were studied
3. Longitudinally unzipped GO nanoribbon showed 30% improvement in antifouling properties compared to pristine PES membrane
4. Optimum loading of GO and GNP to maximize flux and rejection was as low as 0.1 wt.% in the membrane
5. Graphene-based nanocomposite membranes demonstrated promising results for the treatment of oil sands produced water